Sana'a University Journal of Applied Sciences and Technology ISSN : 2958-9568
Vol. 1| No. 2 | Page 208 – 216 | 2023 | https://journals.su.edu.ye/index.php/jast

The Effect of Tartaric Acid Concentration on the Structural, Morphological and Optical Properties of CuO-Fe_2O_3-MgO Nanocomposite

Hisham Alnahari[1,*], A.H. Al-Hammadi[1], Annas Al-Sharabi[2], Adnan Alnehia[1,2]
[1] Department of Physics, Faculty of Science, Sana'a University, Sana'a, Yemen
[2] Department of Physics, Faculty of Applied Sciences, Thamar University, Dhamar, Yemen
***Corresponding author**: his.alnahari@su.edu.ye

Article Info.
Article history:
Received: January 27, 2023
Accepted: April 10, 2023
Published: April 30 2023

Keywords
1. CuO-Fe2O3-MgO
2. Nanocomposite
3. Optical
4. Sol-gel
5. Tartaric acid

ABSTRACT: In the present study, the sol-gel method has been utilized to synthesize tri-phase CuO-Fe_2O_3-MgOnanocomposites (NCs) by employing tartaric acid (TA) as an organic fuel. The obtained NCs were characterized using XRD, SEM, FTIR, and UV-Vis. The XRD pattern asserted the formation of NCs with MgO (cubic), CuO (monoclinic), and Fe_2O_3 (hexagonal) crystals. The crystallite size (D_{av}) was calculated by Scherrer's formula, whereas the optical properties were assessed using UV-Vis spectra. The optical band gap values of the synthesized materials displayed variations related to tartaric acid concentration due to the quantum confinement of tri-metal oxide NCs. The SEM described the morphological properties and FTIR confirmed the formation of interfaces among the metal oxides CuO, Fe_2O_3 and MgO in the NCs. The enhanced optical properties of these tri-metal oxide NCs make them a good candidate for optoelectronic applications.

Contents

1. Introduction

During the last decade, much attention has been focused on metallic oxide nanocomposite materials due to their unique structural, optical, thermal, and antibacterial properties [1-3].

Practically, nanocomposites (NCs) have been created through the mixing of two, three, or more oxides on a nanometer scale [1]. In addition to the favored properties of the NCs, the concentration of each oxide in the mixture may govern the final properties of the NCs [4]. NCs can be fabricated by different methods, such as solution combustion [2], ultrasonic-assisted [5], microwave-assisted [6], sonochemical [4], and chemical co-precipitation routes [7, 8]. Among these, the

sol–gel technique is fast, easy, and low-cost [9]. NCs are potentially suitable for different applications like fuel and solar cells, battery materials, biomedicine, photovoltaic devices, UV-detectors, and gas sensors [7, 10-12]. The interaction between varied oxides with matching band potentials leads to charge separation efficiency, increased charge transferability, and carrier lifetime [12]. Copper oxide (CuO) has prime properties with low-cost preparation. It is a *p*-type semiconductor, has a narrow energy bandgap ranging between 1.2 and 1.8 eV, and, is non-toxic [13-15]. More recently, CuO has been used in certain applications such as electrode material in Li-ion batteries, super capacitors, photocatalytic activity, solar cells, and gas sensing [1, 16]. Magnesium oxide (MgO) is considered a virtual dielectric material. It has unique physicochemical properties, a large bandgap (7.8 eV), high surface reactivity, high adsorption capacity, and is a highly ionic compound [1, 4, 17]. Maghemite (γ-Fe_2O_3) is an *n*-type semiconductor. It has prime properties, such as a favorable optical bandgap (~2.1 eV), non-toxicity, low cost, high biocompatibility, natural abundance, chemical stability, and high magnetic behavior [18-20]. Furthermore, Fe_2O_3 is used in many applications involving sensors, cosmetics, diagnostics, biomedicine, radiology, vaccines, and anti-pathogens [8, 21]. The interaction of CuO, MgO, and Fe_2O_3 significantly alters the physical characteristics of the constituent oxides and enhances the antimicrobial/photocatalytic responses. Moreover, multiphase double heterojunction NCs like ZnO-Yb_2O_3-Pr_2O [22], CdO–NiO–ZnO [23], ZnO–V_2O_5–WO [7], CuO–MgO–ZnO [1], and CuO/α-Fe_2O_3/γ-Al_2O_3 [24] have been prepared and studied for antibacterial and photocatalysis applications. A great deal of interest by researchers has been made to explore the preparation of the pristine oxides CuO, Fe_2O_3 and MgO and their binary nanocomposites [12, 20, 25, 26]. *Selvi et al.* (2021) synthesized CuO/MgO nanocomposites formed by the sol-gel synthesis method. Their results show that the composition is found to be highly crystalline in nature and of higher purity. No secondary phase or impurity peaks are noticed in all the composites, indicating that the required nanocomposites can be easily synthesized using the sol-gel method [12]. CuO/MgO nanocomposite prepared by facile chemical co-precipitation by Pricilla *et al.* (2021). XRD analysis confirms the formation of a CuO/MgO nanocomposite, and the bandgap value of the prepared composite is determined to be 1.67 eV [27]. Boroujeni *et al.* (2019) prepared CuO-Fe_2O_3 using a Schiff base complex as a precursor through a solid-state thermal decomposition method. Spherical particles of the nanocomposite (20-30 nm) were obtained. The bandgap of a superparamagnetic nanocomposite was estimated to be 4.2 eV [28]. In this work, CuO-Fe_2O_3-MgO NCs were synthesized for the first time via a sol-gel method using tartaric acid as a fuel.

Tartaric acid is a common organic acid that can be easily obtained from natural sources such as grapes and tamarind. It has low toxicity. Tartaric acid can be used as a precursor for the synthesis of various nanomaterials such as metal oxides, carbon-based materials, and metal nanoparticles. Additionally, tartaric acid has functional groups that can act as reducing agents or stabilizers during the synthesis of nanomaterials. Therefore, it is possible that researchers chose tartaric acid as a fuel due to its availability, renewability, low toxicity, and functional groups that aid in the synthesis of nanomaterials [29-33]. Tartaric acid plays an important role in the formation of nanomaterials by acting as a reducing agent, chelating agent, and stabilizer. Its unique

chemical properties make it an attractive candidate for use in various nanomaterial synthesis methods**.** The structural, optical, and morphological properties of the as-prepared CuO-Fe_2O_3-MgO NCs were investigated.

2-Materials and Method

2.1 Materials

Mg $(NO_3)_2.6(H_2O)$ (BDH, 97%), $Fe(NO_3)_3.9(H_2O)$ (Sigma–Aldrich, 97%), Cu $(NO_3)_2.6(H_2O)$ (Sigma–Aldrich, 98%), distilled water (DW), and tartaric acid were used without further purification.

2.2. Synthesis Protocol

The sol-gel route [34] has been used to prepare the target tri-phase metal oxides, CuO-Fe_2O_3-MgO NCs, at various concentrations of TA, as detailed below.

2.2.1. Preparation of the Salt Solutions

Cu $(NO_3)_2.6(H_2O)$ (2.54 g in 15mLDW), Fe $(NO_3)_3.9(H_2O)$ (4.24 g in 15mLDW), and Mg $(NO_3)_2.6(H_2O)$ (2.69 g in 15mLDW) with a constant molar ratio (1:1:1) were fabricated as three separate solutions. The salt solutions were first separately stirred for 15 minutes at room temperature to obtain a homogeneous solution, then mixed together and further homogenized for 30 minutes at room temperature to obtain solution X.

2.2.2. Synthesis of CuO-Fe_2O_3-MgO Nanocomposites Using Tartaric Acid

At first, 3g of TA (1M) was dissolved in 20 mL of DW and stirred for 15 minutes. This solution was designated as solution Y. After that, solutions X and Y were mixed in a 200-mL beaker and stirred for 1.5 hrs at 90°C until obtaining a dried mass of CuO-Fe_2O_3-MgO. The product was calcined at 800 °C for 90 minutes. The NCs were then designated as T1. Similar steps were used to prepare 1.5T and 2T while using 1.5 and 2 M TA, respectively.

2.3 Characterization Techniques

UV-Vi's spectrophotometer (Hitachi U3900 with the software of Varian Cary 50), X-Ray Diffraction (XRD) (Shimadzu EDX-720) X-ray diffractometer with Cu Kα radiation (λ= 0.154 nm), SEM (JSM-6360, Japan), and FTIR (Bruker Tensor 27, range 400–4000 cm^{-1}).

3. Results and Discussion

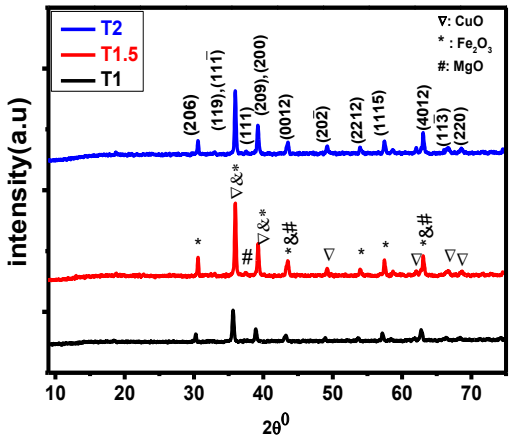

Figure 1. X-ray diffraction of CuO-Fe_2O_3-MgO nanocomposite

3.1 XRD Analysis

Figure 1 illustrates the X-ray diffraction patterns of CuO-Fe_2O_3-MgO NCs at different concentrations of TA (1, 1.5 and 2M) and equimolar precursors. The XRD patterns have shown three types of particles, CuO-Fe_2O_3-MgO, for all the synthesized samples. Observed diffraction patterns of oxides displayed that CuO is monoclinic, Fe_2O_3 is tetragonal, and MgO is cubic in phase structures. The peaks of angle 2θ = 32.413, 35.582, 56.748, 58.411, 61.807, 66.362, and 68.326 correspond to (110), (11$\bar{1}$), (0 2 1), (20$\bar{2}$), (11$\bar{3}$), (3 1 0), and (220) planes of CuO.

These peaks are in good agreement with ICSD: 48-1548. The Fe_2O_3 peaks appeared at 30.296, 33.957, 38.863, 43.237, 53.759, and 62.76 compared to the reflections of planes (2 0 6), (1 0 9), (2 0 9), (0 0 12), (2 2 12), and (4 0 12), respectively. They correspond to ICSD:

25-1402. The peaks at 2θ = 36.931, 43.303, and 62.445, corresponding to the (111), (331), and (220) planes of MgO, are in good agreement with ICSD: 45-0946. It is evident to note that there were no other peaks for impurity that could be detected. The average crystallite size (*D*) was evaluated from Debye Scherrer's formula as follows: $D = \frac{0.9\lambda}{\beta cos\theta}$; where λ is the wavelength of XRD, β is the line broadening at FWHM and θ is Bragg's $angle$ [23, 35]. Due to the importance of the density of dislocation ($\boldsymbol{\delta}$) in the mechanical and structural properties of materials, it was evaluated for the synthesized NCs as well. The computed values of the average size (*D*) and the density of dislocation ($\boldsymbol{\delta}$) are gathered in Table 1. The $\boldsymbol{\delta}$ was computed via the equation $\boldsymbol{\delta} = {}^{1}/_{D^2}$[36]. From Table 1, the results show that the average crystallite size increases as the TA concentration increases. The increase in crystallite sizes is attributed to the small dislocation density value because of the inverse relation between dislocation density parameters and crystallite size. According to the XRD data obtained, an increase in the TA concentration leads to a change or increase in the intensity of peaks in the XRD pattern and an increase in the size of crystallites, as shown in Table 1. This

result leads to the presence of additional distortions and vacancies in the structure. In addition, the increase in fuel leads to an increase in impurities formed from the spontaneous combustion process. The increase in TA concentration leads to an increase in the amount of fuel available for combustion, which can cause the particles to grow in size. In addition, excess fuel can lead to the formation of large agglomerates. Therefore, the concentration of TA plays an important role in determining the size and morphology of nanoparticles synthesized by the sol-gel method.

Table 1. Average crystallite and dislocation density of CuO-Fe_2O_3-MgO NCs

samples	CuO	Fe_2O_3	MgO	CuO	Fe_2O_3	MgO
	Average crystallite size(nm)			Dislocation density*10^{14} ($1/m^2$)		
T1	57.48	38.89	21.78	3.03	6.61	2.11
T1.5	67.78	47.43	105.45	2.18	4.45	0.89
T2	93.55	47.16	83.54	1.14	4.49	1.43

3.2 SEM Analysis

Figure 2 displays SEM images of sample T2 at different magnifications. Generally, agglomerated particles were more visible. However, nanoparticle phases and shapes are still identifiable and countable at the nanoscale.

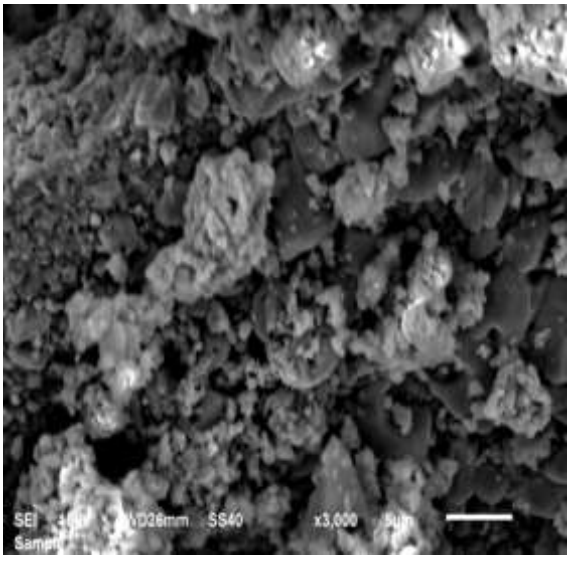

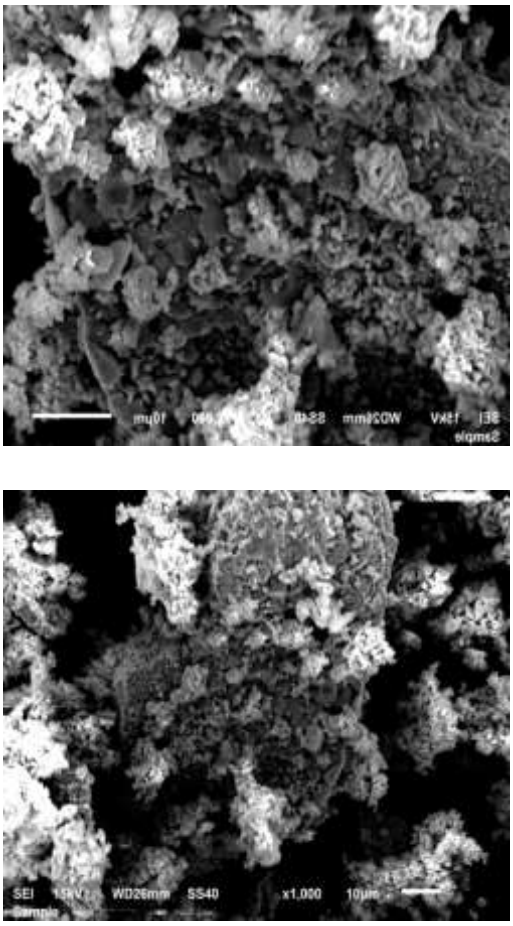

Figure 2. SEM images of sample T2 at

different magnifications

3.3 UV-Visible Analysis

The optical properties of the CuO-Fe_2O_3-MgO NCs were measured via UV–visible spectroscopy. Figure 3 exhibits the absorption spectrum of CuO-Fe_2O_3-MgO NCs in the range of 200–900 nm. From Figure 3, it can be seen that absorption spectra decrease with the increase in the wavelength (λ). Figure 4 shows the transmittance spectrum of CuO-Fe_2O_3-MgO NCs, which suggests that the transmittance of the prepared compounds increases as the TA concentration increases. The coefficient of absorption (α) as a function of the wavelength for all the fabricated compounds is shown in Figure 5. It shows that the α of all the prepared compounds decrease as the wavelength increases. The extinction coefficient (k) is an important optical parameter that illustrates the energy loss due to the scattering and absorption that occur via the molecules and particles found in the material. Figure 6 illustrates the extinction coefficient (k) that increases as the wavelength increases. The optical parameters k and α can be computed as follows: $\alpha = \frac{(2.303A)}{t}$, $k = \frac{\alpha\lambda}{4\pi}$; where A is the absorbance and t is the thickness [3, 23].

Tauc's equation for direct transition [36, 37] was used to compute the optical energy band gap (E_g), which is 3.51, 3.36, and 3.0eV for the CuO-Fe_2O_3-MgO NCs at three different concentrations of TA code, coded as T1, T1.5, and T2, respectively, as shown in Figure 7. These values lie in between CuO (1.8eV), Fe_2O_3 (2 eV), and MgO (7.8 eV), which make CuO-Fe_2O_3-MgO NCs suitable for optoelectronic applications. Furthermore, it is observed that the decrease in photon energy occurs with an increment in the concentration of TA. This indicates that the use of TA as fuel in the combustion process significantly affects the optical properties of the products. Moreover, it is well known that under some circumstances, oxygen atoms can move or leave the metal oxide crystal lattice, leaving oxygen vacancies. According to the XRD data mentioned above, the distribution and average particle size have a significant impact on the physicochemical characteristics of the samples. In addition, it is well known that particle surface area increases with particle size. As the density of oxygen vacancies increases, ion transport, and especially oxygen transport, destroys the original particles. This shows that the defects increased as particle size decreased, which combined the influences of crystalline size and surface defects. The surface oxygen vacancies played a role in separating photogenerated charges in the nanocomposite, thus reducing the band gap energy values as particle size increased [38, 39].

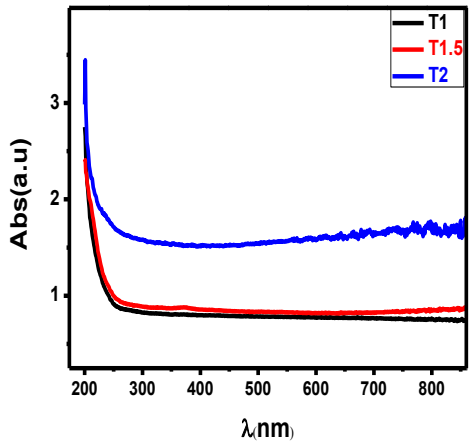

Figure 3. The absorption spectrum of CuO-Fe_2O_3-MgO nanocomposite

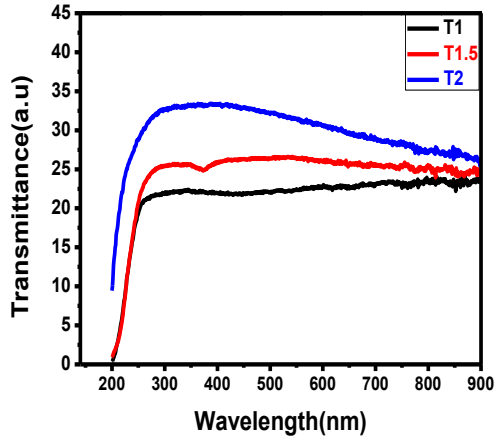

Figure 4. The transmittance spectrum of CuO-Fe_2O_3-MgO nanocomposite

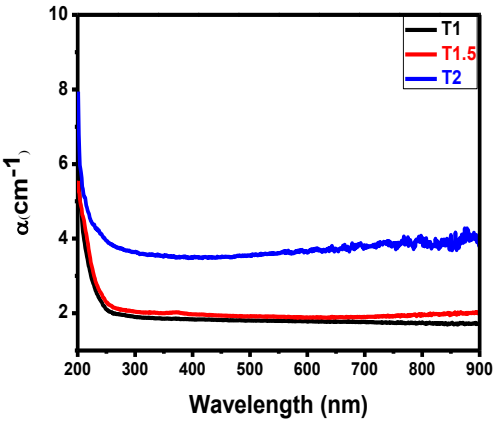

Figure 5. The coefficient of absorption (α) as a function of the wavelength

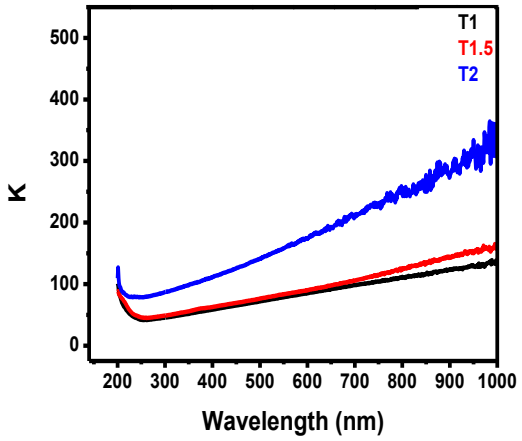

Figure 6. The coefficient of extinction (k) as function of the wavelength

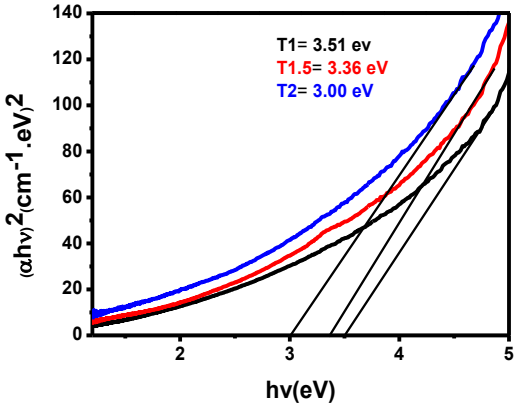

Figure 7. The optical energy band gap for CuO-Fe_2O_3-MgO nanocomposite

3.4 FTIR Analysis

FTIR analysis is used to explore chemical bonding as well as functional groups of grown CuO-Fe_2O_3-MgONCs in the range of 400 to 4000cm^{-1}, as shown in Figure 8. The vibrational bands of metal oxides were visible in the region 400-869 cm^{-1} [7]. The band at 1446.6cm^{-1} is attributed to C–C stretching vibrations [1]. The broad peaks at 1632 and 3470 cm^{-1} are attributed to the hydroxyl group [40]. The change in intensity and shifting of peaks are due to structural defects and lattice distortions, which confirm the formation of an

interface among CuO, Fe_2O_3, and MgO in the NCs.

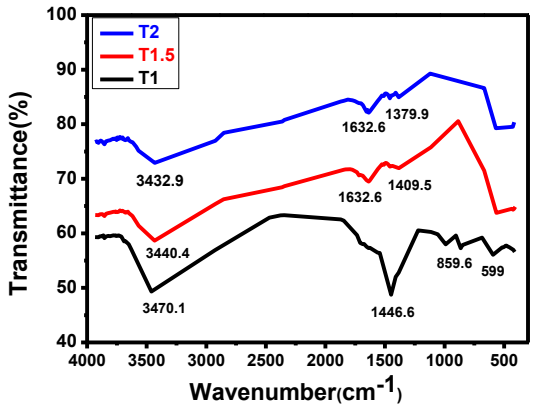

Figure8. FTIR spectraof CuO-Fe_2O_3-MgO nano-composite

4. Conclusion

CuO-Fe_2O_3-MgONCs were successfully prepared via the sol-gel technique. The characteristic properties of the various prepared NCs under different TA concentrations support their impact on the final crystallite size of NCs. The optical bandgap (E_g) of the prepared samples was found to be decreased as the TA concentration increased. These results could indicate the usefulness of the application of TA for tailoring the properties of the targeted triphasic metal-oxide NCs, a method that can be enhanced further with further optimization.

Funding

No fund was received.

Acknowledgements

The authors would like to thank Mr. Ahmed Al-Khalqi for his support during optical measurements.

Conflicts of Interest

The authors declare no conflicts of interest.

5. References

[1] T. Munawar, F. Mukhtar, S. Yasmeen, M. Naveed-ur-Rehman, M.S. Nadeem, M. Riaz, M. Mansoor, F. Iqbal, Sunlight-induced photocatalytic degradation of various dyes and bacterial inactivation using CuO–MgO–ZnO nanocomposite, Environmental Science and Pollution Research, 28 (2021) 42243-42260.

[2] J. Kulkarni, R. Ravishankar, H. Nagabhushana, K.S. Anantharaju, R.B. Basavaraj, M. Sangeeta, H.P. Nagaswarupa, Structural, Optical and Photocatalytic Properties of MgO/CuO Nanocomposite Prepared by a Solution Combustion Method Materials Today: Proceedings, 4 (2017) 11756–11763.

[3] A. Al-Sharabi, K.S.S. Sada'a, A. AL-Osta, R. Abd-Shukor, Structure, optical properties and antimicrobial activities of MgO–$Bi_{2-x}Cr_xO$ nanocomposites prepared via solvent-deicient method, Scientiic Reports, 12 (2022) 10647.

[4] N.H. Deepthi, Y.S. Vidya, K.S. Anantharaju, R.B. Basavaraj, D. Kavyashree, S.C. Sharma, H. Nagabhushana, Optical, electrical and luminescent studies of CuO/MgOnanocomposites synthesized via sonochemical method, Journal of Alloys and Compounds 786 (2019) 855-866.

[5] K. Karthik, S. Dhanuskodi, C. Gobinath, S. Prabukumar, S.Sivaramakrishnan, Ultrasonic-assisted CdO–MgO nanocomposite for multifunctional applications, Materials technology, 34 (2019) 403-414.

[6] V. Revathi, K. Karthik, Microwave assisted CdO–ZnO–MgO nanocomposite and its photocatalytic and antibacterial studies, Materials Science: Materials in Electronics 29 (2018) 18519–18530.

[7] F. Mukhtar, T. Munawar, M.S. Nadeem, M.N.u. Rehman, M. Riaz, F. Iqbal, Dual S-scheme heterojunction ZnO–V_2O_5–WO nanocomposite with enhanced photocatalytic and antimicrobial activity, Materials Chemistry and Physics 263 (2021) 124372.

[8] A. Azhari, M.S. Sh, F. Golestanifard, A. Saberi, Phase evolution in Fe_2O_3/MgO nanocomposite prepared via a simple precipitation method, Materials Chemistry and Physics 124 (2010) 658–663.

[9] S.e. Leroy, J.-F. Blach, A. Kopia, S. Lech, Ł. Cieniek, N. Kania, e. Saitzek, Enhancement of photocatalytic properties of nanosized $La_2Ti_2O_7$ synthesized by glycine-assisted sol-gel route Journal of Photochemistry & Photobiology, A: Chemistry, 426 (2022) 113739.

[10] S. Vignesh, A.L. Muppudathi, J.K. Sundar, Multifunctional performance of gC_3N_4–$BiFeO_3$–CuO_2 hybrid nanocomposites for magnetic separable photocatalytic and antibacterial activity, Materials Science:

Materials in Electronics 31 (2020) 13998-13999.
[11] Emre Alp, Halil Eşgin, M.Kürşat Kazmanlı, A. Genç, Synergetic activity enhancement in 2D CuO-Fe_2O_3nanocomposites for the photodegradation of rhodamine B, Ceramics International, 45 (2019) 9174–9178.
[12] K.T. Selvi, K.A. Mangai, M. Priya, S. Sagadevan, Enhanced electrical and magnetic properties of CuO/MgO nanocomposites, Chemical Physics Letters 765 (2021) 138320.
[13] K. Phiwdang, S. Suphankij, W. Mekprasart, W. Pecharapa, Synthesis of CuO Nanoparticles by Precipitation Method Using Different Precursors Energy Procedia, 34 (2013) 740-745.
[14] M.E. Grigore, E.R. Biscu, A.M. Holban, M.C. Gestal, A.M. Grumezescu, Methods of Synthesis, Properties and Biomedical Applications of CuO Nanoparticles, Pharmaceuticals 9(2016) 75.
[15] H. Alnahari, A.H. Al-Hammadi, A. Al-Sharabi, A. Alnehia, A.-B. Al-Odayni, Structural, morphological, optical, and antibacterial properties of CuO–Fe_2O_3–MgO–$CuFe_2O_4$nanocomposite synthesized via auto-combustion route, Journal of Materials Science: Materials in Electronics, 34 (2023) 682.
[16] H. Absike, M. Hajji, H. Labrim, A. Abbassi, H. Ez-Zahraouy, Electronic, electrical and optical properties of Ag doped CuO through modified BeckeJohnson exchange potential, Superlattices and Microstructures, 127 (2019) 128-138.
[17] T. Baysal, N. Noor, A. Demir, Nanofibrous MgO composites: structures, properties, and applications, Polymer-Plastics Technology and Materials, 59 (2020) 1522-1551.
[18] N.A. Yazdi, M.R. Arefi, E. Mollaahmadi, B.A. Nejand, To study the effect of adding Fe_2O_3 nanoparticles on the morphology properties and microstructure of cement mortar, Life Science Journal, 8 (2011) 550-554.
[19] M. Farahmandjou, F. Soflaee, Synthesis and Characterization of α-Fe_2O_3Nanoparticles by Simple CoPrecipitation Method, Phys. Chem. Res, 3 (2015) 191-196.
[20] R. Ramesh, V. Yamini, D. Rajkumar, S.J. Sundaram, D. Lakshmi, F.L.A. Khan, Biogenic synthesis of □- Fe_2O_3 nanoparticles using Plectranthus amboinicus leaf extrac, Materials Today: Proceedings, 36 (2020) 453-458.
[21] M.M. Alam, H.B. Balkhoyor, A.M. Asiri, M.R. Karim, M.T.S. Chani, M.M. Rahman, Fabrication of ascorbic sensor acid with Co_3O_4.Fe_2O_3 nanosphere materialsby electrochemical technique, Surfaces and Interfaces, 20 (2020) 100607.
[22] T. Munawar, S. Yasmeen, M. Hasan, K. Mahmood, A. Hussain, A. Ali, M.I. Arshad, F. Iqbal, Novel tri-phase heterostructured ZnO–Yb_2O_3–Pr_2O nanocomposite; structural, optical, photocatalytic and antibacterial studies, Ceramics International, 46 (2020) 11101-11114.
[23] T. Munawar, F. Iqbal, S. Yasmeen, K. Mahmood, A. Hussain, Multi metal oxide NiO-CdO-ZnO nanocomposite–synthesis, structural, optical, electrical properties and enhanced sunlight driven photocatalytic activity, Ceramics International, 46 (2020) 2421-2437.
[24] A. Kanwal, S. Sajjad, S.A.K. Leghari, Z. Yousaf, Cascade electron transfer in ternary CuO/α-Fe_2O_3/γ-Al_2O_3nanocomposite as an effective visible photocatalyst Journal of Physics and Chemistry of Solids 151 (2021) 109899.
[25] M. Sun, Y. Lei, H. Cheng, J. Ma, Y. Qin, S. Komarneni, Y. Kong, R. A, Mg doped CuO-Fe_2O_3 composites activated by persulfate as highly active heterogeneous catalysts for the degradation of organicpollutants, Journal of Alloys and Compounds, 825 (2020) 154036.
[26] G. Balakrishnan, R. Velavan, K.M. Batoo, E.H. Raslan, Microstructure, optical and photocatalytic properties of MgO nanoparticles, Results in Physics 16 16 (2020) 103013.
[27] R.B. Pricilla, A.S. Elsie, A. Mohan, V.M. Kumar, B. Vidhya, R. Nandhakumar, Studies on the structural, optical and photocatalytic properties of CuO/MgO nanocomposite prepared by facile chemical co-precipitation, Materials Today: Proceedings, 47 (2021) 837-842.
[28] K.P. Boroujeni, Z. Tohidiyan, H. Shahsanaei, Synthesis and characterization of Fe_2O_3/CuO nanocomposite as a new photocatalyst for solar degradation of methylene blue dye in aqueous solution, in: The 27th Iranian Conference on Organic Chemistry, Iran 2019.
[29] V. Meltzer, E. Pincu, Thermodynamic study of binary mixture of citric acid and tartaric acid, Central European Journal of Chemistry, 10 (2012) 1584-1589.

[30] G.H. Kale, A.V. Humbe, P.B. Kharat, D.N.Bhoyar, K.M. Jadhav, Tartaric Acid a Novel Fuel Approach: Synthesis and Characterization of $CoFe_2O_4$ Nano Particles, BIONANO FRONTIER 8(2015).

[31] A.C. Clark, P.D. Prenzler, G.R. Scollary, Impact of the condition of storage of tartaric cid solutions on the production and stability of glyoxylic acid, Food Chemistry, 102 (2007) 905-916.

[32] I.G. Shitu, Z.A. Talib, J.L.Y. Chi, M.M.A. Kechick, H. Baqiah, Influence of tartaric acid concentration on structural and optical properties of CuSe nanoparticles synthesized via microwave assisted method, Results in Physics, 17 (2020) 103041.

[33] I. Begum, S. Shamim, F. Ameen, Z. Hussain, S.A. Bhat, T. Qadri, M. Hussain, A Combinatorial Approach towards Antibacterial and Antioxidant Activity Using Tartaric Acid Capped Silver Nanoparticles, Processes, 10 (2022) 716.

[34] Z. T.Khodair, T. M.Al-Saadi, A.H. Abed, Effect of Fuel on the Structural and Optical Properties of MgO Nanoparticles Prepared by Auto–Combustion of Sol-Gel Method, Advances in physics theories and applications, 60 (2016).

[35] A. Al-Sharabi, A. Alnehia, A.H. Al-Hammadi, K.A. Alhumaidha, A. AL-Osta, The effect of Nigella sativa seed extract concentration on crystal structure, band gap and antibacterial activity of ZnS-NPs prepared by green route, J Mater Sci: Mater Electron, 33 (2022) 20812-20822.

[36] A. AL-Osta, A. Alnehia, A.A. Qaid, H.T. Al-Ahsab, A. Al-Sharabi, Structural, morphological and optical properties of Cr doped ZnS nanoparticles prepared without any capping agent, Optik - International Journal for Light and Electron Optics, 214 (2020) 164831.

[37] A. Alnehia, A.-B. Al-Odayni, A. Al-Sharabi, A.H. Al-Hammadi, W.S. Saeed, Pomegranate Peel Extract–Mediated Green Synthesis of ZnO-NPs: Extract Concentration-Dependent Structure, Optical, and Antibacterial Activity, Journal of Chemistry, 2022 (2022) 1-11.

[38] D. Li, H. Song, X. Meng, T. Shen, J. Sun, W. Han, X. Wang, Effects of particle size on the structure and photocatalytic performance by alkali-treated TiO_2, Nanomaterials, 10 (2020).

[39] A.L. Kozlovskiy, M.V. Zdorovets, The study of the structural characteristics and catalytic activity of $Co/CoCo_2O_4$ nanowires, Composites Part B 191 (2020) 107968.

[40] A. Alnehia, A. Al-Sharabi, A.H. Al-Hammadi, A.-B. Al-Odayni, S.A. Alramadhan, R.M. Alodeni, Phyto-Mediated Synthesis of Silver-Doped Zinc Oxide Nanoparticles from Plectranthus barbatus Leaf Extract: Optical, Morphological, and Antibacterial Properties, Biomass Conversion and Biorefinery, (2023).